CHEMISTRY
A EUROPEAN JOURNAL

Competition between Superexchange-Mediated and Sequential Electron Transfer in a Bridged Donor–Acceptor System

Mikael U. Winters, Karin Pettersson, Jerker Mårtensson, and Bo Albinsson*[a]

Abstract: The temperature- and solvent-dependence of photoinduced electron-transfer reactions in a porphyrin-based donor–bridge–acceptor (DBA) system is studied by fluorescence and transient absorption spectroscopy. Two competing processes occur: sequential and direct superexchange-mediated electron transfer. In a weakly polar solvent (2-methyltetrahydrofuran), only direct electron transfer from the excited donor to the appended acceptor is observed, and this process has weak temperature dependence. In polar solvents (butyronitrile and dimethylformamide), both processes are observed and the sequential electron transfer shows strong temperature dependence. In systems where both electron transfer processes are observed, the long-range superexchange-mediated process is more than two times faster than the sequential process, even though the donor–acceptor distance is significantly larger in the former case.

Keywords: electron transfer · porphyrin · sequential electron transfer · solvent effects · superexchange

Introduction

Long-range electron transfer has been a field of intense research for several decades. It plays a major role in many interesting areas such as natural and artificial photosynthesis[1–4] and molecular electronic devices.[5–8] Many aspects of electron transfer have been covered over the years, for example, its dependence on parameters such as temperature, free energy, orientation, and distance. Electron transfer is considered to be long-range if the electron travels more than 10 Å and the distances are often much longer. Over these distances it is energetically more favorable for the electron to tunnel through unoccupied orbitals of the intervening medium than to travel through empty space. Such tunneling is usually referred to as a superexchange or through-bond mechanism. Linking a donor–acceptor couple with a suitable bridge provides an electronic medium that effectively facilitates superexchange mediation. Without any bridge mediation, long-range electron transfer would be very unlikely because such a process would have through-space character, which requires direct orbital overlap between the donor and the acceptor. The transition from superexchange-mediated electron transfer to sequential or "hopping" mechanisms has recently become the focus of many researchers.[9–17] In the superexchange case there is a probability for electron transfer owing to a virtual intermediate state, whereas for sequential electron transfer, the electron is temporarily localized and a chemical intermediate is produced. A better understanding of the factors governing the competition between the two mechanisms would be useful in many instances, for example, when discussing electron-transfer processes in native reaction centers or molecular wire behavior.[18–20]

Much attention has been directed towards the influence of the electronic structure of intervening bridge structures on the effective electronic coupling in geometrically well-defined donor–bridge–acceptor (DBA) systems.[16,21–23] Superexchange-mediated electron transfer in a DBA system directly results in a charge-separated state ($D^{\bullet+}BA^{\bullet-}$), whereas sequential electron transfer in the first step yields an intermediate state, $D^{\bullet+}B^{\bullet-}A$ in which the anion radical of the bridge is formed. By controlling the energy gaps between the primary excited DBA system and the charge-separated species ($D^{\bullet+}B^{\bullet-}A$ and $D^{\bullet+}BA^{\bullet-}$), physical mediation (superexchange) may gradually be turned into chemical mediation, whereby genuine chemical intermediates are realized.

The DBA system studied in this work (Figure 1) consists of a (5-aryl-2,8,12,18-tetraethyl-3,7,13,17-tetramethylpor-

[a] M. U. Winters, K. Pettersson, Dr. J. Mårtensson, Prof. B. Albinsson
Department of Chemistry and Bioscience
Chalmers University of Technology
412 96 Gothenburg (Sweden)
Fax: (+46) 31-772-3858
E-mail: balb@chembio.chalmers.se

Supporting information for this article is available on the WWW under http://www.chemeurj.org/ or from the author.

DOI: 10.1002/chem.200400755

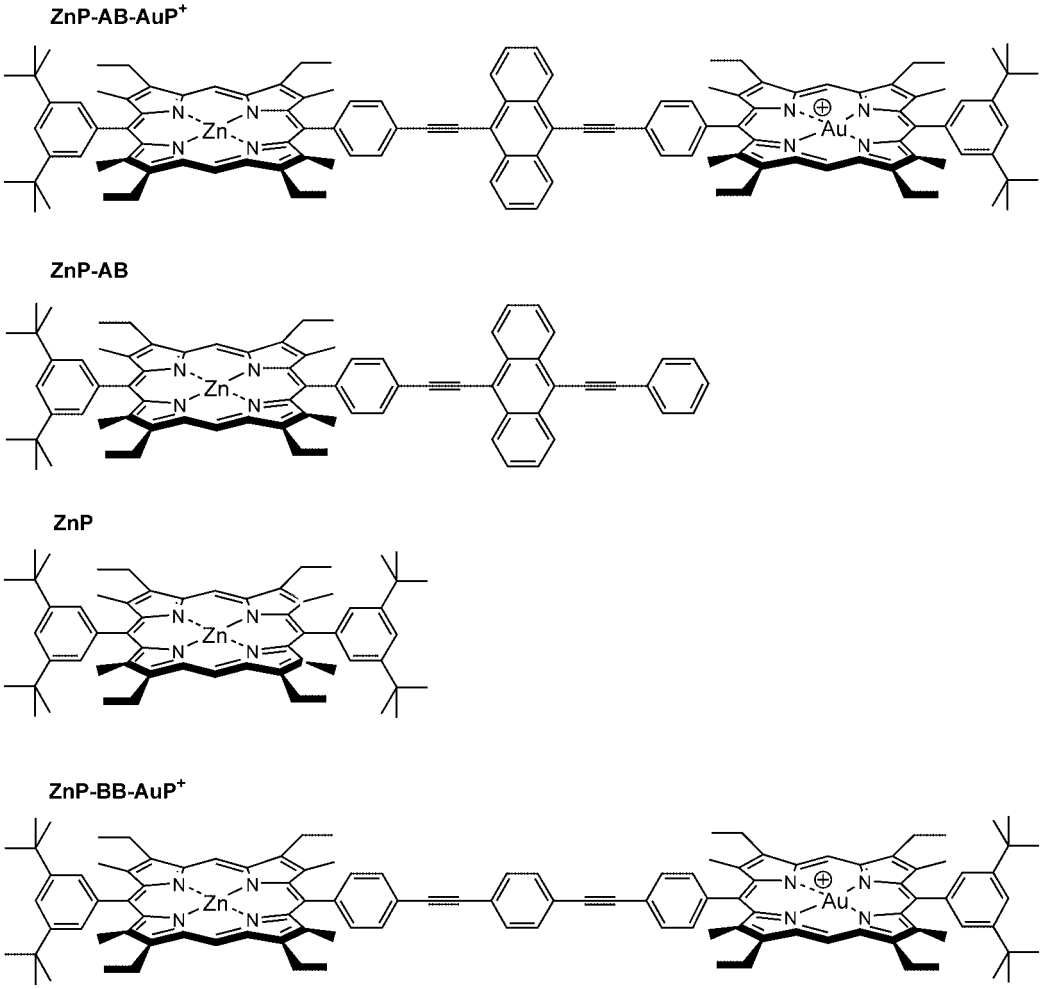

Figure 1. The molecules studied: the **ZnP-AB-AuP$^+$** triad, the **ZnP-AB** dyad, the unsubstituted **ZnP** donor, and the **ZnP-BB-AuP$^+$** triad.

phyrin-15-yl)zinc (**ZnP**) covalently linked by a 9,10-bis(phenylethynyl)anthracene (**AB**) bridge to its corresponding gold(III) porphyrin (**AuP$^+$**). It is part of an ongoing project concerned with the influence of the bridging chromophore on photoinduced energy- and electron-transfer processes in a series of DBA systems.[16,24–32] The main interests of the present study include the influences of temperature and solvent polarity on the electron-transfer properties of **ZnP-AB-AuP$^+$**, and, in particular, the competition between sequential and superexchange mechanisms, which is schematically described in Figure 2. The intermediate created from a sequential electron transfer in this system is **ZnP$^{\cdot+}$-AB$^{\cdot-}$-AuP$^+$**. This charge-separated species forms **ZnP$^{\cdot+}$-AB-AuP$^{\cdot}$** in a second step, the same species that is formed from direct superexchange-mediated electron transfer. Comparisons have been made with the triad **ZnP-BB-AuP$^+$** (Figure 1), in which the porphyrins are linked by 1,4-bis(phenylethynyl)-benzene (**BB**). This system will form a charge-separated state only by superexchange-mediated electron transfer when excited[16] because it has no possibility of sequential electron transfer, and it is therefore a useful reference substance.

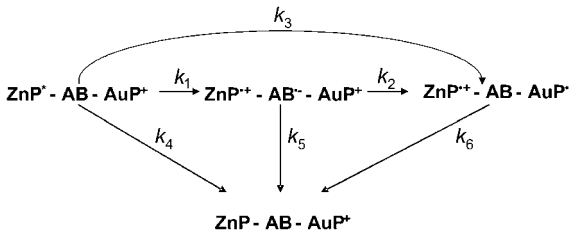

Figure 2. The proposed kinetic model: the excited **ZnP** donor is deactivated by two competing parallel electron-transfer mechanisms, one of which is sequential and one that is superexchange-mediated.

Results

The aim of the present work has been to determine the effects of solvent polarity and temperature on the electron-transfer processes of **ZnP-AB-AuP$^+$**, and to understand the competition between sequential and superexchange-mediated electron transfer in this system. Three solvents of varying polarity were used in the study: 2-methyltetrahydrofuran (2-MTHF), butyronitrile (BuCN), and *N*,*N*-dimethylformamide

(DMF). The emission properties of the system, which have been examined by steady-state fluorescence measurements and time-correlated single-photon counting experiments, will be presented foremost in this section. This is followed by a discourse on the excited-state dynamics, which were studied by means of femtosecond transient absorption. In the discussion that follows, it will be deduced that donor quenching is caused by two competing electron-transfer pathways.

Ground-state absorption: **ZnP-AB-AuP$^+$** consists of three separate chromophores, as demonstrated in Figure 3, where it is indicated that a linear combination of the monomer

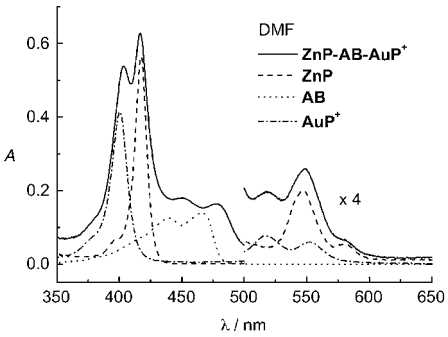

Figure 3. Ground-state absorption spectra of **ZnP-AB-AuP$^+$** (——), **ZnP** (-----), **AB** (•••••), and **AuP$^+$** (–•–•) in DMF. The right-hand side of the Figure is enlarged four times.

(**ZnP**, **AB**, and **AuP$^+$**) absorption spectra is similar to the triad spectrum.[33] In the Q-band region ($\lambda > 500$ nm), **ZnP** has its maximum absorption at 545 and 580 nm, whereas **AuP$^+$** has its maximum absorption at 510 and 560 nm. Furthermore, in the Soret band (~400 nm), the **ZnP** maximum absorption is at 415 nm, whereas **AuP$^+$** has its peak maximum at 400 nm. The absorption profiles are similar for all three solvents used in this study (2-MTHF, BuCN, and DMF), although the absorption maxima are shifted a few nanometers (±5 nm).

Emission properties: Figure 4 shows the temperature dependence of the zinc porphyrin fluorescence quantum yield (Φ_f) in 2-MTHF, BuCN, and DMF, for the unsubstituted donor **ZnP**, the dyad **ZnP-AB** and the triad **ZnP-AB-AuP$^+$**. The quantum yield of **ZnP** is approximately 2.3% at room temperature in all solvents, but increases somewhat as the temperature decreases. Interestingly, the donor emission of **ZnP-AB** is considerably quenched in the polar solvents (BuCN, DMF, Figure 4b,c) compared with **ZnP**, in contrast to the less polar solvent (2-MTHF, Figure 4a) where the quantum yields are similar to those of **ZnP** itself.[33] Moreover, the quantum yield of the donor in **ZnP-AB-AuP$^+$** is lower than that for both **ZnP** and **ZnP-AB** in all solvents at all temperatures. It will be demonstrated that in the less polar solvent (2-MTHF) only superexchange-mediated elec-

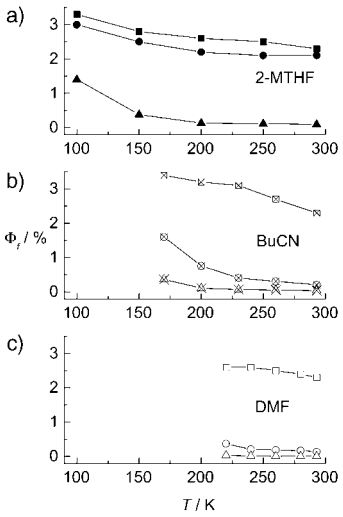

Figure 4. Fluorescence quantum yield for **ZnP** (squares), **ZnP-AB** (circles), and **ZnP-AB-AuP$^+$** (triangles) in a) 2-MTHF (filled symbols), b) BuCN (crossed symbols), and c) DMF (open symbols).

tron transfer from **ZnP** to **AuP$^+$** quenches the donor fluorescence, whereas in the polar solvents (BuCN, DMF) two competing quenching mechanisms are responsible for the quenching (Figure 2), that is, sequential and direct electron transfer.

The fluorescence lifetimes of the zinc porphyrin donor (**ZnP**) in different systems and at different temperatures in either of the solvents are given in Tables 1–3. Estimates of the lifetimes are given for both the unsubstituted donor (τ_D) and the donor in the presence of bridge and bridge–acceptor (τ_{DB} and τ_{DBA}, respectively). In Equations (1a)–(1c) the observed lifetimes are expressed in the rate constants presented in Figure 2.

Table 1. Fluorescence lifetimes for **ZnP** (τ_D), **ZnP-AB** (τ_{DB}), and **ZnP-AB-AuP$^+$** (τ_{DBA}) in 2-MTHF, as well as the calculated quenching efficiencies (E) and rates (k).

T [K]	τ_D [ns]	τ_{DB} [ns]	τ_{DBA}[a] [ps]	E_{DBA}[b] [%]	k_3[c] [s^{-1}]
295	1.48	1.36	61±3.7	95.9	1.6×10^{10}
255	1.54	1.41	57±1.3	96.3	1.7×10^{10}
215	1.63	1.45	60±0.78	96.3	1.6×10^{10}
175	1.74	1.37	89±2.3	94.9	1.1×10^{10}
135	1.89	1.69	120±4.3	93.7	7.8×10^{9}
100	2.02	–[d]	140±3.1	93.1	6.6×10^{9}

[a] In general, the errors are very small and thus estimates are only given where it is judged that they are relevant. [b] Equation (2b). [c] Equation (3c).[33] [d] Not determined.

$$\tau_D = (k_{ic} + k_{isc} + k_f)^{-1} = (k_4)^{-1} \quad (1a)$$

$$\tau_{DB} = (k_4 + k_1)^{-1} \quad (1b)$$

$$\tau_{DBA} = (k_4 + k_1 + k_3)^{-1} \quad (1c)$$

Table 2. Fluorescence lifetimes for **ZnP** (τ_D), **ZnP-AB** (τ_{DB}), and **ZnP-AB-AuP$^+$** (τ_{DBA}) in BuCN, as well as the calculated quenching efficiencies (E) and rates (k).

T [K]	τ_D [ns]	τ_{DB} [ps]	τ_{DBA} [ps]	E_{DB} [%]	E_{DBA} [%]	k_1 [s^{-1}]	k_3 [s^{-1}][a]	$k_1 + k_3$ [s^{-1}]
295	1.52	87	28	94.3	98.2	1.1×10^{10}	2.4×10^{10}	3.5×10^{10}
270	1.58	102	32	93.5	97.9	9.2×10^{9}	2.1×10^{10}	3.0×10^{10}
245	1.60	135	44	91.7	97.3	6.8×10^{9}	1.5×10^{10}	2.2×10^{10}
220	1.61	204	59	87.3	96.4	4.3×10^{9}	1.2×10^{10}	1.6×10^{10}
195	1.66	342	79	79.4	95.3	2.3×10^{9}	0.98×10^{10}	1.2×10^{10}
170	1.69	652	96	61.4	94.3	9.4×10^{8}	0.89×10^{10}	0.98×10^{10}

[a] Equation (3b). See Table 1 for additional comments.

Table 3. Fluorescence lifetimes for **ZnP** (τ_D), **ZnP-AB** (τ_{DB}), and **ZnP-AB-AuP$^+$** (τ_{DBA}) in DMF, as well as the calculated quenching efficiencies (E) and rates (k). k_1 is the rate constant for the sequential electron-transfer process and k_3 for the superexchange-mediated electron-transfer process.

T [K]	τ_D [ns]	τ_{DB} [ps]	τ_{DBA} [ps]	E_{DB} [%]	E_{DBA} [%]	k_1 [s^{-1}]	k_3 [s^{-1}][a]	$k_1 + k_3$ [s^{-1}]
295	1.61	57	21	96.5	98.7	1.7×10^{10}	3.0×10^{10}	4.7×10^{10}
280	1.64	67	23	95.9	98.6	1.4×10^{10}	2.8×10^{10}	4.2×10^{10}
265	1.67	80	27	95.2	98.4	1.2×10^{10}	2.5×10^{10}	3.7×10^{10}
250	1.69	100	35	94.1	98.0	9.4×10^{9}	1.9×10^{10}	2.8×10^{10}
235	1.72	130	44	92.4	97.4	7.1×10^{9}	1.5×10^{10}	2.2×10^{10}
220	1.76	180	62	89.8	96.5	5.0×10^{9}	1.0×10^{10}	1.5×10^{10}

[a] Equation (3b). See Table 1 for additional comments.

solvents (BuCN, DMF). This is another indication that a temperature-dependent process occurs that is only active in polar solvents. Second, τ_{DBA} is considerably shorter than τ_D and τ_{DB} in all solvents at all temperatures. This shows that a second mechanism, that is, superexchange-mediated electron transfer, is active in both polar and nonpolar solvents.

Tables 4–6 present the corresponding results from measurements on **ZnP-BB-AuP$^+$**, for which electron transfer only occurs by the superexchange mechanism.[16] The electron-transfer rate for this system is one order of magnitude slower than for **ZnP-AB-AuP$^+$**, and at low temperatures additional quenching attributed to excita-

In the present situation, fluorescence quenching is attributed to more than one process. It has been assumed that the two quenching processes—sequential electron transfer (k_1) and superexchange-mediated electron transfer (k_3)—are independent and additive. This is based on the reasonable first approximation that the presence of **AuP$^+$** does not appreciably affect the rate of the first step of the sequential mechanism. The rate constant k_1, as measured in the corresponding DB system, **ZnP-AB**, is thus unchanged in **ZnP-AB-AuP$^+$** and the overall quenching rate of this system equals the sum of the two rates involved ($k_1 + k_3$). The quenching efficiencies, E_{DB} and E_{DBA}, as well as the relevant rate constants are then easily calculated from the fluorescence lifetimes [Eq. (2) and (3)].

$$E_{DB} = 1-\tau_{DB}/\tau_D \quad (2a)$$

$$E_{DBA} = 1-\tau_{DBA}/\tau_D \quad (2b)$$

$$k_1 = (\tau_{DB})^{-1}-(\tau_D)^{-1} \quad (3a)$$

$$k_3 = (\tau_{DBA})^{-1}-(\tau_{DB})^{-1} \quad (3b)$$

$$k_1 + k_3 = (\tau_{DBA})^{-1}-(\tau_D)^{-1} \quad (3c)$$

The results from the lifetime measurements are in complete agreement with the quantum yield measurements. First, τ_D and τ_{DB} are approximately equal in 2-MTHF[33] (Table 1), whereas in the polar solvents (Table 2, Table 3) τ_{DB} is significantly shorter than τ_D. The lifetimes τ_D and τ_{DB} in 2-MTHF are relatively insensitive to temperature, whereas τ_{DB} increases with decreasing temperature in the polar

Table 4. Fluorescence lifetimes (τ_{DBA}), quenching efficiencies (E_{DBA}), and rates for quenching (k_3) of **ZnP-BB-AuP$^+$** in 2-MTHF.

T[K]	τ_{DBA}[ps]	E_{DBA}[a][%]	k_3[b][s^{-1}]
295	500	66.2	1.3×10^{9}
255	560	63.6	1.1×10^{9}
215	548	66.4	1.2×10^{9}
175	560	67.8	1.2×10^{9}
135	970	48.7	4.8×10^{8}
100	1300	35.6	2.5×10^{8}

[a] Equation (2b). [b] Equation (3b). The rate constant for excitation energy transfer, calculated from the Förster equation, is 2×10^{8} s^{-1}.

Table 5. Fluorescence lifetimes (τ_{DBA}), quenching efficiencies (E_{DBA}), and rates for quenching (k_3) of **ZnP-BB-AuP$^+$** in BuCN.

T[K]	τ_{DBA}[ps]	E_{DBA}[a][%]	k_3[b][s^{-1}]
295	290	80.9	2.7×10^{9}
270	410	74.0	1.7×10^{9}
245	435	72.8	1.6×10^{9}
220	510	68.3	1.3×10^{9}
195	680	59.0	7.9×10^{8}
170	840	50.3	5.2×10^{8}

[a] Equation (2b). [b] Equation (3b). The rate constant for excitation energy transfer, calculated from the Förster equation, is 0.8×10^{8} s^{-1}.

tion energy transfer cannot be neglected in this system. The contribution from energy transfer has been calculated from the Förster equation.

The temperature dependence of the rates of the two involved electron-transfer processes are presented in Figure 5. In this context, it is useful to compare the two triads **ZnP-BB-AuP$^+$** and **ZnP-AB-AuP$^+$**. The fact that charge transfer

Table 6. Fluorescence lifetimes (τ_{DBA}), quenching efficiencies (E_{DBA}), and rates for quenching (k_3) of **ZnP-BB-AuP$^+$** in DMF.

T[K]	τ_{DBA}[ps]	E_{DBA}[a][%]	k_3[b][s^{-1}]
295	320	80.1	2.4×10^9
280	360	78.0	2.1×10^9
265	410	75.4	1.8×10^9
250	470	72.2	1.5×10^9
235	560	67.4	1.1×10^9
220	690	60.8	8.3×10^8

[a] Equation (2b). [b] Equation (3b). The rate constant for excitation energy transfer, calculated from the Förster equation, is $0.6\times10^8\ s^{-1}$.

in **ZnP-BB-AuP$^+$** proceeds *only* by superexchange allows a specific comparison of the solvent and temperature dependence of the superexchange-mediated electron transfer. Initially, however, consider the slopes of the lines in Figure 5

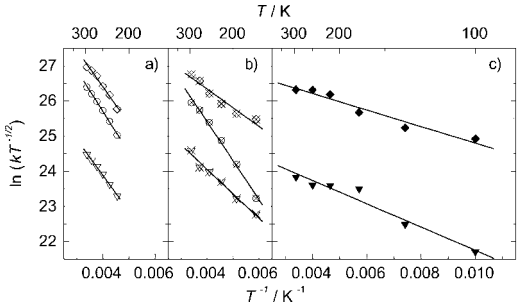

Figure 5. Temperature dependence of the rate constants (k_1 (circles), k_3 in **ZnP-AB-AuP$^+$** (diamonds), and k_3 in **ZnP-BB-AuP$^+$** (triangles)) in a) DMF, b) BuCN, and c) 2-MTHF. k_1 is the rate constant for the sequential electron-transfer process and k_3 for the superexchange-mediated process.

that represent the *sequential* mechanism in **ZnP-AB-AuP$^+$**. Changing the solvent slightly affects the magnitude of the rate, but it does not affect its pronounced temperature dependence. However, if the same comparison is made between the lines representing the superexchange-mediated electron transfer in **ZnP-AB-AuP$^+$** (Figure 5a–c), it can be seen that changing the solvent does not only affect the magnitude but surprisingly also the temperature dependence of this mechanism. **ZnP-BB-AuP$^+$** now offers a possibility to determine whether this is in fact a property of this mechanism in the investigated solvents or a result of the initial assumption that the electron-transfer processes are independent. By changing the bridge moiety, the strength of the electronic coupling of the system is changed,[16] and this should affect the magnitude of the quenching rate but *not* the effects of temperature (i.e. the slopes of the lines in Figure 5). An examination of Figure 5 shows that this is indeed true: the slopes of the lines representing the quenching caused by superexchange are the same for the two triads; however, the strong solvent dependence remains in the **ZnP-BB-AuP$^+$** system. The reasons for this behavior will be discussed below.

In summary, the emission properties of the investigated systems strongly suggest two competing mechanisms. The first mechanism, which is sequential electron transfer, is inactive in nonpolar solvents and displays strong temperature dependence once active. The superexchange-mediated process is active in both polar and nonpolar solvents and exhibits a temperature dependence that differs between the solvents. In the next section, experimental data is presented that strengthens this hypothesis further.

Femtosecond transient absorption measurements: Transient absorption measurements were performed in all three solvents to verify the existence of the radicals in the proposed reaction scheme (Figure 2) and to make conclusions regarding charge separation and recombination kinetics. Presented in this section are the experiments performed in DMF; however, control experiments performed in BuCN confirmed that the system exhibits the same kind of kinetics in these two solvents at room temperature. In contrast, experiments in 2-MTHF were different, signaling the absence of a sequential electron-transfer mechanism. The transient differential absorption spectra in Figure 6 and Figure 7 show characteristic spectral features of the excited states of **ZnP-AB** and **ZnP-AB-AuP$^+$**, respectively. The zinc porphyrin excited states absorb strongly ($S_1\rightarrow S_n$ and $T_1\rightarrow T_n$) in the 430–

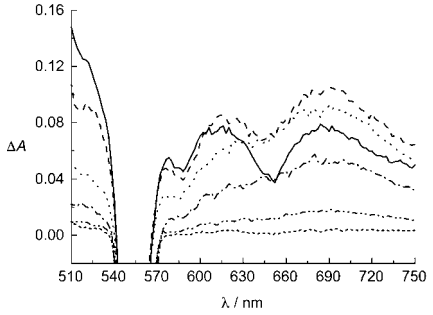

Figure 6. Transient absorption spectra of **ZnP-AB** in DMF: 5 ps (——), 15 ps (– – –), 55 ps (•••••), 95 ps (–•–•), 150 ps (··–), and 250 ps (-----) after the excitation pulse (λ_{ex} = 549 nm).

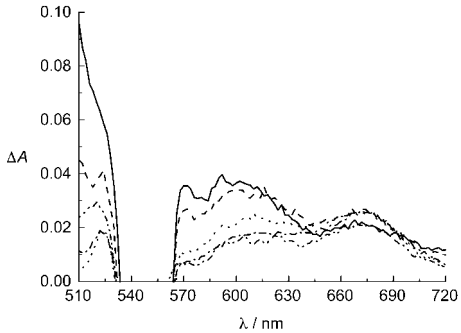

Figure 7. Transient absorption spectra of **ZnP-AB-AuP$^+$** in DMF: 5 ps (——), 15 ps (– – –), 150 ps (•••••), 250 ps (–•–•), and 1400 ps (··–) after the excitation pulse (λ_{ex} = 549 nm).

530 nm region with a tail extending above 600 nm.[30] There are two visible contributions from bleach bands in the spectra that are assigned to ground-state absorption, one at 549 nm, which is the wavelength used to excite the sample (Q(1,0) transition), and one at about 580 nm, which is the Q(0,0) transition. Furthermore, there is an expected bleach component at 510 nm assigned to gold porphyrin ground-state absorption, which is not as obvious, and also two negative bands assigned to stimulated emission at 580 and 640 nm. The gold porphyrin moiety absorbs approximately 20–25% of the excitation light at the wavelength used (Figure 3) and thus there are also gold porphyrin excited states in the spectra. ^{1}**AuP*** undergoes intersystem crossing very rapidly (~240 fs) and with unity yield forms the first excited triplet state ^{3}**AuP***, which has strong absorption at about 600 nm.[34]

The zinc porphyrin radical cation, which is produced by intramolecular electron transfer, has an absorption band centered at 680 nm.[35–37] The presence of a strong signal in this region is a clear indication that deactivation of the excited state is caused by electron transfer. Another important key to the electron transfer kinetics would be the detection of the **AB** radical anion that is produced by a sequential mechanism and thus spectroelectrochemical experiments were made to determine the spectral signature of this species. The experiment shows that the **AB** anion has a fairly broad band centered at 630 nm ($\varepsilon \sim 4\times10^4\,\mathrm{M^{-1}cm^{-1}}$) and also a weaker band at 820 nm (Figure S1, Supporting Information).

Figure 6 shows that the differential transient absorption of **ZnP-AB** disappears almost completely in about 250 ps. The absorption in the 500 nm region decays single exponentially, whereas above 590 nm it exhibits a rise-time as well as a single exponential decay. The interpretation is that the charge-separated species **ZnP**$^{\cdot+}$**-AB**$^{\cdot-}$ is being built up by electron transfer from the excited zinc porphyrin. Comparing Figures 6 and 7, it is clear that the absorption in the region around 600 nm relative to that above 640 nm is stronger for **ZnP-AB-AuP**$^+$ than for **ZnP-AB**. This is attributed to the presence of excited states of the gold porphyrin. Therefore, it is no longer possible to say whether there is any build-up resulting from the formation of the **AB** anion or the **ZnP** cation radical because the ^{3}**AuP*** absorption is quite strong and builds up immediately. Above 640 nm it is possible to see a clear rise-time that also corresponds to the decay of the $S_1 \rightarrow S_n$ absorption of the zinc porphyrin, and at long delay times there remains an absorption attributed to the fully charge-separated state **ZnP**$^{\cdot+}$**-AB-AuP**$^{\cdot}$.

The dynamics of **ZnP-AB** and **ZnP-AB-AuP**$^+$ at 690 nm, a wavelength where absorption is expected from the **ZnP** radical cation as well as the **AB** radical anion with little interference from other species, are illustrated in Figure 8a and b, respectively. The kinetic trace of **ZnP-AB** displays a rise-time of about 20 ps and decays single exponentially in approximately 55 ps. It is already known from single-photon counting measurements that the donor fluorescence lifetime in DMF is 57 ps at room temperature (Table 3). The consistency of the data therefore demand that what at first glance seems to be a decay, must be identified as the building up of the **ZnP** radical cation, and this is thus a case of "inverted kinetics" ($k_5 > k_1$, Figure 2). This result indicates that the concentration of the radicals (**AB**$^{\cdot-}$ and **ZnP**$^{\cdot+}$) will be quite low at all times. It should also be noted that there are no long-lived states present in the **ZnP-AB** case. The corresponding measurement on the triad (Figure 8b), on the other hand, also shows a long lifetime, indicative of the charge-separated state **ZnP**$^{\cdot+}$**-AB-AuP**$^{\cdot}$. In this case, it is expected that the concentration of **ZnP**$^{\cdot+}$ is higher than that of the **AB** radical anion at all times and, thus, it may be difficult to experimentally detect **AB**$^{\cdot-}$ in the triad. However, since the transient trace at this wavelength (Figure 8b) is the sum of the absorption of the two transient species **ZnP**$^{\cdot+}$ and **AB**$^{\cdot-}$, the presence of **ZnP**$^{\cdot+}$**-AB**$^{\cdot-}$**-AuP**$^+$ can be deduced from the shape of the decay. If the absorption in this region was attributable to only one long-lived species (e.g. **ZnP**$^{\cdot+}$) the decay profile would be flat. On the other hand, if the bridge anion radical, which also absorbs at this wavelength (Figure S1, Supporting Information), is formed and its transient absorption kinetics has a profile similar to the one in Figure 8a and that profile is added to a flat one, the result is a decay trace similar to that observed (Figure 8b). It can thus be concluded that the anion radical is indeed present. This result indicates that the sequential and superexchange-mediated electron transfer act in parallel in this system (vide infra). The rise-time of the trace is 14 ps, which is in reasonable agreement with the donor fluorescence lifetime. The rate of recombination cannot be determined exactly on the timescale used in this experiment, but it may be concluded that it is longer than 5 ns; earlier results indicate that it is most probably shorter than 15 ns.[26]

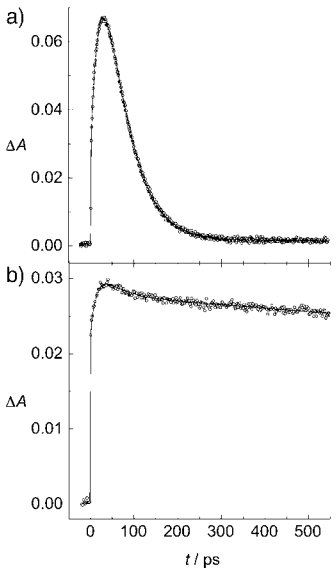

Figure 8. Kinetic traces of a) **ZnP-AB** and b) **ZnP-AB-AuP**$^+$ recorded in DMF at 690 nm. The sample was excited at 549 nm.

Figure 9 shows the **ZnP-AB-AuP**$^+$ kinetic trace at 500 nm, where, at short times, primarily the excited state ab-

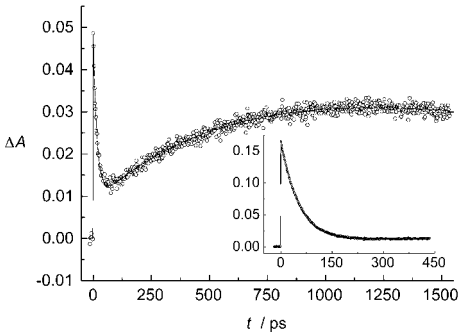

Figure 9. Transient absorption kinetics of **ZnP-AB-AuP$^+$** in DMF at 500 nm. The inset shows the corresponding trace for **ZnP-AB**. Both samples were excited at 549 nm.

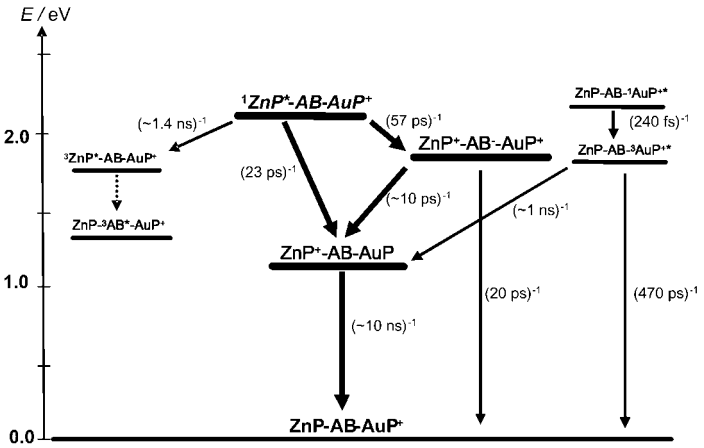

Figure 10. Energy diagram and rates (at room temperature in DMF) for the species that may be involved in the post-excitation processes.

sorption of **^{1}ZnP*** is probed and the inset at the low right of the figure shows **ZnP-AB** transient absorption at the same wavelength. The differential absorption of **ZnP-AB** decays in approximately 50 ps, which is in good agreement with the previous experiments. It also confirms that charge separation of **ZnP-AB** is in fact slower than charge recombination, giving rise to inverted kinetics. The transient absorption of the **ZnP-AB-AuP$^+$** system shows a more complex behavior. The curve has a prompt rise, as expected, and there is an initial fast decay of 15 ps in accord with the rise-time of the 690 nm absorption and the fluorescence decay. The curve then displays a slow absorption build-up (in approximately 1 ns) followed by the decay associated with recombination. The build-up is probably attributable to ground-state recovery of the gold porphyrin moiety, which takes place on this timescale,[26,34] or possibly attributable to the formation of **^{3}AB***.

Discussion

The aim of this work has been to identify and quantify two competing electron-transfer mechanisms in a DBA system, schematically outlined in Figure 2. This has been carried out by varying the solvent temperature and polarity in a number of fluorescence studies, as well as by transient absorption measurements. The two competing processes are superexchange-mediated electron transfer and a sequential electron-transfer mechanism, which generates an anthryl radical anion intermediate. Previous work has identified that a stepwise electron-transfer mechanism is responsible for the additional donor quenching observed in **ZnP-AB** and **ZnP-AB-FeP** and investigated its dependence upon solvent polarity and coordination.[30,31] Also, a switching behavior based on coordination effects was demonstrated.

It is informative to construct the energy-level diagram of the system as it provides some insight into the activity of the various pathways in a thermodynamic framework. The energies of the involved charge-separated states have been calculated in the three solvents used, of which DMF has been given a more detailed presentation (Figure 10). The energy of the 0–0 transitions ($E_{0\text{–}0}$) were determined from ground-state absorption (Figure 3) and emission spectra, whereas the energy gaps between the **ZnP** first excited state and the charge-separated states were calculated from redox potentials with the Weller equation [Eq. (4)].[39]

$$\Delta G^o = e(E_{ox}-E_{red})-\mathrm{E}_{0-0} + \frac{e^2}{4\pi\varepsilon_0}\left(\frac{1}{\varepsilon_S(T)}-\frac{1}{\varepsilon_{ref}}\right)\left(\frac{1}{2R_D}+\frac{1}{2R_A}\right)-\frac{e^2}{4\pi\varepsilon_S(T)\varepsilon_{ref}R_{DA}} \quad (4)$$

E_{ox} and E_{red} are the donor and acceptor oxidation and reduction potentials, respectively, determined by cyclic voltammetry,[40] ε_S is the dielectric constant of the solvent and ε_{ref} the dielectric constant of the solvent in which the electrochemical measurements were performed. R_D and R_A are the average radii of the donor and acceptor, which are set to 4.8 Å for the porphyrin moieties[41] and 8 Å for the **AB** unit. The **ZnP**/**AuP$^+$** center-to-center distance (R_{DA}) is approximately 25.3 Å and the **ZnP**/**AB** center-to-center distance in the **ZnP-AB** system is approximately 13.2 Å (estimated from MM$^+$-and PM3-optimized structures, respectively).[27,30] The last term of Equation (4) represents a correction for the Coulombic stabilization between the charge-separated species. This term has been neglected for the superexchange-mediated electron transfer, because this process has the nature of a charge shift, and furthermore, this term is quite small (0.1 eV or less) for the large donor–acceptor distance in this case.

Figure 10 shows that two electron-transfer pathways are thermodynamically possible from **^{1}ZnP*-AB-AuP$^+$**. First, the **ZnP$^{\cdot+}$-AB$^{\cdot-}$** state is energetically close to the **^{1}ZnP*** state and secondly, there is a large driving force to produce the charge-shifted state **ZnP$^{\cdot+}$-AB-AuP$^{\cdot}$**. Figure 10 also raises interesting questions about other processes that may or may not be active. It was previously mentioned that **AuP$^+$** excited states are necessarily involved in the relaxation dynamics and that **^{3}AuP*** is produced very rapidly with 100% yield. It has been shown that this state is capable of

hole-transfer in similar systems.[26] Another pathway that might be of interest is the formation of the excited triplet state of the bridging chromophore, ^{3}**AB***. However, hole transfer from the ^{3}**AuP*** state is slow compared to the short-lived states of primary importance and thus the processes originating from this state should be secondary to those of particular interest for this study. Other deactivation mechanisms that might be present, for example, energy transfer, are two orders of magnitude slower[16] and cannot compete with relaxation processes that proceed on the picosecond timescale. In the **ZnP-BB-AuP**$^+$ system, however, part of the donor fluorescence quenching will be caused by excitation energy transfer.[16]

Steady-state fluorescence measurements established that **ZnP-AB** behaves like an electron donor–acceptor couple in polar solvents, whereas in nonpolar solvents the donor is only significantly quenched in the presence of **AuP**$^+$. The quenching efficiency of **ZnP-AB** relative to **ZnP** is as high as 96.5% in DMF and 94.3% in BuCN. On energetic grounds it seems likely that the observed quenching is attributable to an electron-transfer mechanism in view of the fact that the charge-separated species is stabilized to a large extent in polar solvents. This picture was also confirmed by transient absorption measurements in which the zinc porphyrin radical cation was observed. This is strong evidence that donor quenching is indeed attributable to electron transfer. When the gold porphyrin moiety is added to the system, the quantum yield is lowered even more, and the quenching efficiency rises to 98.7% in DMF and 98.2% in BuCN, whereas in 2-MTHF the quenching efficiency is 95.9% (Tables 1–3).

Competition between superexchange-mediated and sequential electron transfer: In the present study, a system has been presented in which, under certain circumstances, a sequential electron-transfer mechanism competes with superexchange-mediated electron transfer. The prerequisite for this is that the solvent is polar enough to stabilize the intermediate radical of the bridge sufficiently for it to act as an electron acceptor. The term sequential electron transfer is not valid, however, if the rate constant of the second step, **AB**$^{\cdot-}$**-AuP**$^+$→**AB-AuP**$^{\cdot}$, is not comparable to that of charge recombination. Although the presence of the **AB** radical anion is indirectly indicated by the observed parallel action of the sequential and direct electron-transfer processes (Figure 8b), the lifetime of this species could not be measured directly. Therefore, simulations of the kinetics were made in order to establish that the observed behavior was consistent with a sequential electron transfer. The approach used was based on solving the master equation for the concentrations of the involved species in the proposed model (Figure 2) and comparing the simulated kinetics to those observed experimentally (in DMF). From the simulations, it was found that the concentration of the **AB** radical anion will be low at all times as a consequence of the fast charge recombination ($k_5 > k_1$, vide supra). In the **ZnP-AB** case, its concentration is equal to that of the **ZnP**$^{\cdot+}$ species, and the concentration will only be approximately 15% of the initial concentration of singlet-excited zinc porphyrin. From kinetic simulations on the triad **ZnP-AB-AuP**$^+$, it was found that the rate for the second electron-transfer step **AB**$^{\cdot-}$**-AuP**$^+$→**AB-AuP**$^{\cdot}$ (k_2) was of the order $(10\ \mathrm{ps})^{-1}$ to correctly fit the observed transient (Figure 8b). Because the recombination reaction (k_5) for the **ZnP-AB** dyad was found to occur in 20 ps (formation in 57 ps) the process is to be considered a sequential mechanism rather than parallel quenching of the singlet-excited **ZnP**. The concentration of **ZnP**$^{\cdot+}$**-AB**$^{\cdot-}$**-AuP**$^+$ is expected to be very low, about 10% of the initial concentration of the **ZnP** excited state, and a direct detection is therefore fairly difficult. Since **ZnP*** and **AB**$^{\cdot-}$ have comparable extinction coefficients, this corresponds to a differential absorption signal of approximately 0.01 (Figure 7), and thus there will be no clear peak from the anion radical in the spectra.

When comparing the values of the rate constants for electron transfer, calculated from single-photon counting data, it is found that the long-range electron transfer is faster than the sequential transfer at all temperatures, although the transfer distance is twice as large. This is attributed to the small driving force for the sequential electron transfer, even in a highly polar solvent, such as DMF, together with the large electronic coupling for superexchange-mediated transfer. It is interesting to compare the ratio between k_3 and k_1 in the two polar solvents. In BuCN, the ratio increases with decreasing temperature. At room temperature, the superexchange-mediated electron transfer is two times faster than the sequential mechanism, whereas it is ten times faster at low temperatures. This is not surprising, since the superexchange-mediated electron transfer in this DBA system is a virtually activation-less process in BuCN, whereas sequential electron transfer, creating a radical intermediate, is a thermally activated process and is thus strongly temperature dependent. In DMF however, this ratio is constant, the direct electron transfer being approximately 2 times faster at *all* temperatures, which implies that both mechanisms exhibit a strong temperature dependence in this solvent (vide infra).

Temperature dependence of the electron-transfer processes: According to the Marcus–Hush theory of diabatic electron transfer, the rate constant for electron transfer in the high temperature limit is given by Equation (5).[42,43]

$$k_{\mathrm{ET}} = \sqrt{\frac{\pi}{\hbar^2 \lambda k_{\mathrm{B}} T}}|V|^2 \exp\left[-\frac{(\Delta G^o + \lambda)^2}{4\lambda k_{\mathrm{B}} T}\right] \qquad (5)$$

where k_{B} is the Boltzmann constant, T the temperature, V the electronic coupling, $\Delta G°$ the driving force [Eq. (4)], and λ the total reorganization energy. Since $\Delta G°$ can be determined experimentally, a fitting of the experimental rate constants to the Marcus equation yields V and λ. The reorganization energies estimated from the experiments can then be compared with theoretical values calculated with the Born dielectric continuum model [Eq. (6)].[39,42–46]

$$\lambda_{Born} = \lambda_i + \lambda_o = \lambda_i + \frac{e^2}{4\pi\varepsilon_0}\left(\frac{1}{2R_D}+\frac{1}{2R_A}-\frac{1}{R_{DA}}\right)\left(\frac{1}{n^2}-\frac{1}{\varepsilon_S}\right) \quad (6)$$

λ_o is the outer reorganization energy, which is estimated by the second term in Equation (6), whereas the inner reorganization energy λ_i is estimated separately for each case. The linear fit of the data in Figure 5 to Equation (5) yielded reasonable results for the **ZnP-AB** system; however, the corresponding fits to the data for the triads gave unrealistic values of the electronic coupling and reorganization energies (not shown). To overcome this difficulty, the temperature dependence of the parameters in the Marcus–Hush theory was considered explicitly.

The redox potentials of the three components have been measured in CH_2Cl_2[16] and from Equation (4) values for $\Delta G°$ in the solvents used for spectroscopy have been determined. For these calculations, as well as for the calculations of reorganization energies, the dielectric properties of the solvents are very important. Because the dielectric constant for some solvents, and in this case particularly that of BuCN and DMF, has pronounced temperature dependence, temperature-dependent functions $\varepsilon(T)$ have been used.[47] The electronic coupling also exhibits a certain dependence on temperature, owing to the rotational freedom of the D-B and D-B-A linkages, which is expected to lower the coupling with decreasing temperature.[32] Viscous effects make this rotation solvent-dependent, which has been considered in order to fully understand the variation found in the electronic coupling.

The experimental data for **ZnP-AB** was fitted by means of three different approaches. The first method was a simple linear regression based on a constant driving force for each solvent [Eq. (4)] and a solvent-independent electronic coupling (treated as a common parameter), which gives an effective electronic coupling between the zinc porphyrin and the bridge moiety of about 50 cm^{-1}. The second method took the temperature dependence of the dielectric properties of the solvents into account (the driving force used was a function of $\varepsilon(T)$),[47] and a better fit was found. This fit for the rate constants k_1 (Figure 11) resulted in a different set of parameters (Table 7), and the electronic coupling was now estimated to be 13 cm^{-1}. Lastly, the third method introduced linear temperature dependence in the electronic coupling; however, this approach failed to improve the fit despite the increased flexibility introduced by a fourth parameter and was therefore considered irrelevant. Table 7 also presents the reorganization energies calculated from Equation (6), assuming the inner reorganization energy to be zero in this case.

The same three approaches were applied to the rate constant k_3, representing the superexchange-mediated electron transfer. Simply fitting the data from the two systems (**ZnP-AB-AuP$^+$** and **ZnP-BB-AuP$^+$**) in the three solvents separately with no common parameters or added solvent properties result either in large variations in the couplings or in unreasonable reorganization energies (cf. Figure 5), and this

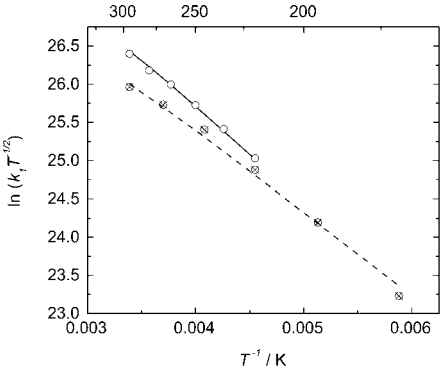

Figure 11. The rate constant for sequential electron transfer, k_1, is fitted to the Marcus equation [Eq. (5)]. The BuCN data is represented with crossed over circles and the fit with a dashed line. The DMF data is represented with empty circles and the fit with a solid line. In the calculations, the electronic coupling is treated as a common parameter, namely, it is equal in both solvents, and the driving force is temperature-dependent.[47]

Table 7. The calculated driving force ($\Delta G°$) and reorganization energies (λ_{Born}), and the reorganization energy (λ) and electronic coupling (V) as determined from experimental data for **ZnP-AB**.

	Sequential electron transfer (k_1)			
Solvent	$\Delta G°(T)$[a] [eV]	λ_{Born}[b] [eV]	λ [eV]	V[c] [cm^{-1}]
BuCN	$\Delta G°$(295 K) = −0.25	0.63	0.56	
	$\Delta G°$(170 K) = −0.18			13
DMF	$\Delta G°$(295 K) = −0.38	0.61	0.56	
	$\Delta G°$(220 K) = −0.29			

[a] $\Delta G°$ is a function of temperature[47]. [b] For the calculated reorganization energy, see Equation (6). [c] V is a common parameter.

method was therefore rejected. By the use of the reorganization energy as a solvent-specific and common parameter of the two systems and making the driving force a function of temperature, the fit was improved and the variation in the electronic coupling was also partly moderated. Good results were also obtained by doing a similar fit (Figure 12) in which the electronic coupling was also treated as a common parameter (Table 8). By requiring the electronic coupling for the two triads to be independent of solvent and at the same time requiring the reorganization energies to be bridge-independent, the best fit in the mathematical sense is not found because the flexibility of the mathematical function is severely limited. However, the fitting parameters (V and λ) extracted from such a global fit are potentially more physically reliable.

An even stronger moderation occurred when the coupling was allowed to vary with temperature and the fitted curves agreed reasonably well with the experimental data. This is a strong indication that solvent/temperature effects are an important factor when discussing the effective electronic coupling of these systems. In the present study, however, the amount of data does not allow detailed mathematical analysis, and furthermore, the systems used are not ideal for such a study. Accordingly, the data summarized in Table 8 are those obtained by the use of a temperature-dependent driv-

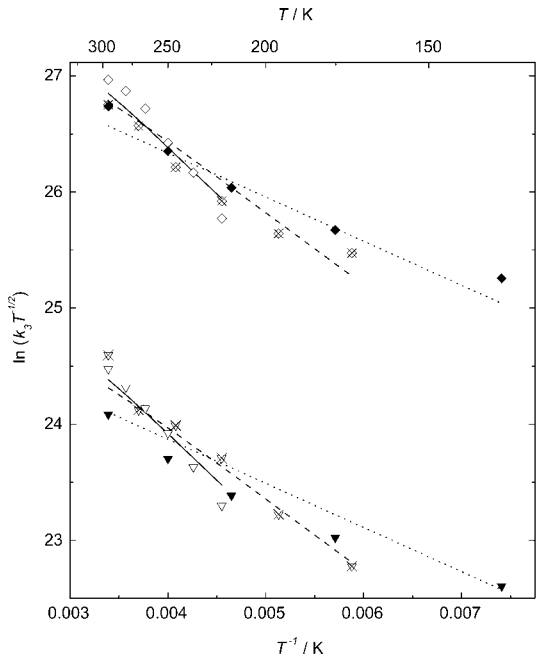

Figure 12. The temperature-dependent rate constant for the superexchange-mediated electron transfer (k_3) fitted to the Marcus equation [Eq. (5)]. The 2-MTHF data is represented with filled diamonds (**ZnP-AB-AuP$^+$**)/triangles (**ZnP-BB-AuP$^+$**) and the fit with a dotted line. The BuCN data is represented with crossed over diamonds (**ZnP-AB-AuP$^+$**)/triangles (**ZnP-BB-AuP$^+$**) and the fit with a dashed line. The DMF data is represented with empty diamonds (**ZnP-AB-AuP$^+$**)/triangles (**ZnP-BB-AuP$^+$**) and the fit with a solid line.

Table 8. The calculated driving force ($\Delta G°$) and reorganization energy (λ_{Born}), and the reorganization energy (λ) and electronic coupling (V) as determined from experimental data for **ZnP-AB-AuP$^+$** and **ZnP-BB-AuP$^+$**.

Solvent	Bridge	Superexchange-mediated electron transfer (k_3) $\Delta G°(T)$[a] [eV]	λ_{Born}[b] [eV]	λ [eV]	V [cm^{-1}][c]
2-MTHF	**ZnP-BB-AuP$^+$**	$\Delta G°$(295 K) = −0.61	1.08	1.02	4.8
	ZnP-AB-AuP$^+$				16
BuCN	**ZnP-BB-AuP$^+$**	$\Delta G°$(295 K) = −0.91	1.37	1.25	4.8
	ZnP-AB-AuP$^+$	$\Delta G°$(170 K) = −0.79			16
DMF	**ZnP-BB-AuP$^+$**	$\Delta G°$(295 K) = −0.96	1.32	1.29	4.8
	ZnP-AB-AuP$^+$	$\Delta G°$(220 K) = −0.88			16

[a] $\Delta G°$ for BuCN and DMF are functions of $\varepsilon(T)$.[47] $\Delta G°$(295 K) was used for 2-MTHF because the temperature range of the available data on this solvent was limited. [b] The calculated reorganization energy [Eq. (6)]. [c] V is common for the respective triad, that is, independent of the solvent.

ing force, but with no assumptions made regarding the solvent control of the effective electronic coupling. Elegant studies have been made with this specific problem in focus.[48,49] For the porphyrin–porphyrin electron-transfer step, the inner reorganization energy is set to 0.2 eV, a value that has been used previously for similar systems,[50] and the Born calculations are in good agreement with the experiments.

For solvents with slow dielectric relaxation, it has been suggested[51] that the electron transfer is governed only by the solvent dynamics, in which case the rate becomes proportional to the inverse solvent relaxation time. The dielectric relaxation times (τ_L, longitudinal dielectric relaxation time) in BuCN and DMF are on the same timescale as the electron transfer in the presented system[52,53] and, more importantly, the τ_L for these solvents increases quite quickly with decreasing temperature, particularly in DMF.[53] This will probably have a pronounced effect on the electron transfer dynamics in **ZnP-AB-AuP$^+$**. Effects of this kind are probably underestimated in many cases and may actually mean that fast electron-transfer processes in DMF, such as the ones studied in this work, can no longer be modeled in the diabatic limit at low temperatures, but rather should be examined theoretically in a solvent-controlled limit. A systematic study of these phenomena would be very interesting, particularly the transition from diabatic to adiabatic conditions.

Conclusion

This work has discussed the competition between superexchange-mediated and sequential electron transfer in a porphyrin-based donor–bridge–acceptor system. By studying how the involved processes depend on solvent polarity and temperature it could be deduced that the electron-transfer processes can be effectively controlled by the choice of medium. Low solvent polarity completely turns off the sequential mechanism. When the two processes are in competition, that is, in polar solvents, the superexchange-mediated electron transfer is about two times as fast as the sequential mechanism, even though the distance for this transfer is twice as long. The temperature-dependent data demonstrated that solvent control of the electron transfer is extremely important and has to be considered explicitly in order for the theoretical models to yield reasonable results. Tentatively, it can also be concluded that since the distribution of possible rotational conformations of the systems narrows with decreasing temperature, the electronic coupling is in fact also temperature-dependent. From the present experiments, however, the magnitude of this effect is not clear. Furthermore, a switching effect based on temperature was demonstrated in BuCN. By lowering the temperature of this solvent, the sequential process is slowed down relative to the superexchange-mediated electron transfer, and eventually it is "turned off".

Experimental Section

Materials: The synthesis of the examined systems as well as the reference compounds have been described in previous publications.[16] All solvents

(2-methyltetrahydrofuran (2-MTHF, $\varepsilon = 6.97$ and $n = 1.405$ at room-temperature) from Acros, butyronitrile (BuCN, $\varepsilon = 24.83$ and $n = 1.382$ at room-temperature) from Merck and *N*,*N*-dimethyl formamide (DMF, $\varepsilon = 38.25$ and $n = 1.430$ at room-temperature) from LabScan) were used as delivered.

Spectroscopic measurements: All measurements were made at room temperature or in a temperature-regulated nitrogen-cooled cryostat (Oxford instruments). Absorption measurements were performed on a Cary 4 Bio spectrophotometer at a 300 nm min^{-1} scan rate and 1 nm bandwidth. Fully corrected steady-state emission spectra were recorded on a SPEX Fluorolog 3 spectrofluorimeter equipped with a xenon lamp. All fluorescence quantum yields were determined relative to **ZnP** in 2-MTHF ($\varphi_f = 0.023$ at room temperature).[27] In order to avoid intermolecular interactions as well as inner filter effects, the absorbance at the excitation wavelength (~545 nm) was kept at 0.05.

Fluorescence lifetimes were determined by means of time-correlated single-photon counting. The sample was excited in the Soret band (~415 nm) by the frequency-doubled output from a mode-locked Ti:sapphire laser (Tsunami, Spectra Physics). A pulse selector (Model 3980, Spectra Physics) was used to achieve a 4 MHz repetition rate. The photons were collected by a microchannel plate photomultiplier tube (MCP-PMT R3809U-50, Hamamatsu) and fed into a multichannel analyzer with 4096 channels yielding a time resolution of $\approx$10 ps (FWHM). A minimum of 10000 counts were recorded in the top channel. The intensity data was fitted by iteratively reconvoluting a three-exponential expression with the instrument response signal with the software package F900 (Edinburgh Instruments). More than one exponential had to be used as the data contained systematic errors caused by reflexes in the cryostat as well as from minute traces of impurities (<0.5%). The artifact disappeared when a regular sample-holder was used and it did not affect the lifetimes of interest. The impurities had lifetimes characteristic of zinc porphyrin, and in the fittings their time constants were therefore set to the lifetimes determined from the corresponding measurements on **ZnP**.

Transient absorption spectra on the femtosecond timescale were recorded by means of the pump–probe technique. The sample was excited at 549 nm with a 1 kHz repetition rate with the sum frequency of the pump and idler from an OPA (TOPAS, Light Conversion Ltd.) pumped by a Ti:sapphire regenerative amplifier (Spitfire, Spectra Physics) producing 110 fs pulses. The amplifier was pumped by a frequency-doubled diode-pumped Nd:YLF laser (Evolution-X, Spectra Physics) and seeded by a Tsunami. A more detailed description of this system is found elsewhere.[38] The kinetic traces were recorded with step sizes between 0.05 and 2 ps, whereas the spectra were recorded with a 2 nm step size. The sample was held in a 1 mm path length cuvette and the optical density was $\approx$1. The recorded traces were fitted individually and globally to a sum of exponentials with the software package MATLAB.

Acknowledgement

This work was supported by grants from the Swedish Science Research Council (VR), the Knut and Alice Wallenberg Foundation, and the Hasselblad Foundation. Reiner Lomoth at the Department of Physical Chemistry at Uppsala University is gratefully acknowledged for his valuable help with the spectroelectrochemical measurements.

[1] D. Gust, T. A. Moore, A. L. Moore, *Acc. Chem. Res.* **2001**, *34*, 40–48.
[2] G. Kodis, P. A. Liddell, L. de la Garza, P. C. Clausen, J. S. Lindsey, A. L. Moore, T. A. Moore, D. Gust, *J. Phys. Chem. A* **2002**, *106*, 2036–2048.
[3] D. Kuciauskas, P. A. Liddell, S. Lin, T. E. Johnson, S. J. Weghorn, J. S. Lindsey, A. L. Moore, T. A. Moore, D. Gust, *J. Am. Chem. Soc.* **1999**, *121*, 8604–8614.
[4] M. R. Wasielewski, *Chem. Rev.* **1992**, *92*, 435–461.
[5] V. Balzani, *Photochem. Photobiol. Sci.* **2003**, *2*, 459–476.
[6] V. Balzani, A. Credi, M. Venturi, *ChemPhysChem* **2003**, *4*, 49–59.
[7] P. Ball, *Nature* **2000**, *406*, 118–120.
[8] A. K. Burrell, M. R. Wasielewski, *J. Porphyrins Phthalocyanines* **2000**, *4*, 401–406.
[9] M. Bixon, J. Jortner, *J. Chem. Phys.* **1997**, *107*, 5154–5170.
[10] H. Imahori, K. Tamaki, Y. Araki, Y. Sekiguchi, O. Ito, Y. Sakata, S. Fukuzumi, *J. Am. Chem. Soc.* **2002**, *124*, 5165–5174.
[11] H. Imahori, K. Tamaki, Y. Araki, T. Hasobe, O. Ito, A. Shimomura, S. Kundu, T. Okada, Y. Sakata, S. Fukuzumi, *J. Phys. Chem. A* **2002**, *106*, 2803–2814.
[12] R. J. Willemse, J. J. Piet, J. M. Warman, F. Hartl, J. W. Verhoeven, A. M. Brouwer, *J. Am. Chem. Soc.* **2000**, *122*, 3721–3730.
[13] J. Springer, G. Kodis, L. de la Garza, A. L. Moore, T. A. Moore, D. Gust, *J. Phys. Chem. A* **2003**, *107*, 3567–3575.
[14] E. G. Petrov, V. May, *J. Phys. Chem. A* **2001**, *105*, 10176–10186.
[15] C. Lambert, G. Noll, J. Schelter, *Nat. Mater.* **2002**, *1*, 69–73.
[16] K. Kilså, J. Kajanus, A. N. Macpherson, J. Mårtensson, B. Albinsson, *J. Am. Chem. Soc.* **2001**, *123*, 3069–3080.
[17] W. B. Davis, W. A. Svec, M. A. Ratner, M. R. Wasielewski, *Nature* **1998**, *396*, 60–63.
[18] F. C. Grozema, Y. A. Berlin, L. D. A. Siebbeles, *J. Am. Chem. Soc.* **2000**, *122*, 10903–10909.
[19] Y. A. Berlin, A. L. Burin, M. A. Ratner, *J. Am. Chem. Soc.* **2001**, *123*, 260–268.
[20] W. B. Davis, M. A. Ratner, M. R. Wasielewski, J. Am. Chem. Soc. **2001**, *123*, 7877–7886.
[21] H. Heitele, M. E. Michel-Beyerle, *J. Am. Chem. Soc.* **1985**, *107*, 8286–8288.
[22] P. Finckh, H. Heitele, M. Volk, M. E. Michel-Beyerle, *J. Phys. Chem.* **1988**, *92*, 6584–6590.
[23] T. J. Chow, N. R. Chiu, H. C. Chen, C. Y. Chen, W. S. Yu, Y. M. Cheng, C. C. Cheng, C. P. Chang, P. T. Chou, *Tetrahedron* **2003**, *59*, 5719–5730.
[24] J. Andréasson, J. Kajanus, J. Mårtensson, B. Albinsson, *J. Am. Chem. Soc.* **2000**, *122*, 9844–9845.
[25] J. Andréasson, A. Kyrychenko, J. Mårtensson, B. Albinsson, *Photochem. Photobiol. Sci.* **2002**, *1*, 111–119.
[26] J. Andréasson, G. Kodis, T. Ljungdahl, A. L. Moore, T. A. Moore, D. Gust, J. Mårtensson, B. Albinsson, *J. Phys. Chem. A* **2003**, *107*, 8825–8833.
[27] K. K. Jensen, S. B. van Berlekom, J. Kajanus, J. Mårtensson, B. Albinsson, *J. Phys. Chem. A* **1997**, *101*, 2218–2220.
[28] J. Kajanus, S. B. van Berlekom, B. Albinsson, J. Mårtensson, *Synthesis* **1999**, 1155–1162.
[29] K. Kilså, J. Kajanus, J. Mårtensson, B. Albinsson, *J. Phys. Chem. B* **1999**, *103*, 7329–7339.
[30] K. Kilså, A. N. Macpherson, T. Gillbro, J. Mårtensson, B. Albinsson, *Spectrochim. Acta Part A* **2001**, *57*, 2213–2227.
[31] K. Kilså, J. Kajanus, S. Larsson, A. N. Macpherson, J. Mårtensson, B. Albinsson, *Chem. Eur. J.* **2001**, *7*, 2122–2133.
[32] A. Kyrychenko, B. Albinsson, *Chem. Phys. Lett.* **2002**, *366*, 291–299.
[33] The **ZnP** and **AB** chromophores are not completely separated, but interact to some extent, which is apparent in Figure 3. This is the most probable explanation for the slightly lower fluorescence quantum yield of **ZnP-AB** in 2-MTHF, rather than quenching by electron transfer.
[34] J. Andréasson, G. Kodis, S. Lin, A. L. Moore, T. A. Moore, D. Gust, J. Mårtensson, B. Albinsson, *Photochem. Photobiol.* **2002**, *76*, 47–50.
[35] A. Helms, D. Heiler, G. McLendon, *J. Am. Chem. Soc.* **1992**, *114*, 6227–6238.
[36] A. M. Brun, A. Harriman, V. Heitz, J. P. Sauvage, *J. Am. Chem. Soc.* **1991**, *113*, 8657–8663.
[37] H. Imahori, K. Hagiwara, M. Aoki, T. Akiyama, S. Taniguchi, T. Okada, M. Shirakawa, Y. Sakata, *J. Am. Chem. Soc.* **1996**, *118*, 11771–11782.
[38] K. Pettersson, K. Kilså, J. Mårtensson, B. Albinsson, *J. Am. Chem. Soc.* **2004**, *126*, 6710–6719.
[39] A. Weller, *Z. Phys. Chem. (München Ger.)* **1982**, *133*, 93–98.

[40] The redox potentials of the involved species are: E_{ox}(**ZnP**) = +0.38 V, E_{red}(**AB**) = −1.68 V, E_{red}(**AuP$^+$**) = −1.05 V.[16]
[41] J. M. DeGraziano, A. N. Macpherson, P. A. Liddell, L. Noss, J. P. Sumida, G. R. Seely, J. E. Lewis, A. L. Moore, T. A. Moore, D. Gust, *New J. Chem.* **1996**, *20*, 839–851.
[42] R. A. Marcus, N. Sutin, *Biochim. Biophys. Acta* **1985**, *811*, 265–322.
[43] R. A. Marcus, *Am. J. Phys. JCP* **1956**, *24*, 966–978.
[44] R. A. Marcus, *Can. J. Chem.* **1959**, *37*, 155–163.
[45] R. A. Marcus, *J. Chem. Phys.* **1965**, *43*, 679–701.
[46] D. Rehm, A. Weller, *Ber. Bunsen Ges. Phys. Chem.* **1969**, *73*, 834–839.
[47] $\varepsilon_{BuCN}(T) = 191.53405 - 1.00591 \times T + 0.00147 \times T^2$, $\varepsilon_{DMF}(T) = 153.64 - 0.60367 \times T + 0.71505 \times 10^{-3} \times T^2$. *Handbook of Chemistry and Physics*, 82nd ed., (Ed.: D. R. Lide), CRC Press, Boca Raton, FL, **2001**.
[48] A. M. Napper, I. Read, D. H. Waldeck, R. W. Kaplan, M. B. Zimmt, *J. Phys. Chem. A* **2002**, *106*, 4784–4793.
[49] K. Kumar, I. V. Kurnikov, D. N. Beratan, D. H. Waldeck, M. B. Zimmt, *J. Phys. Chem. A* **1998**, *102*, 5529–5541.
[50] A. Harriman, V. Heitz, J. P. Sauvage, *J. Phys. Chem.* **1993**, *97*, 5940–5946.
[51] H. Heitele, M. E. Michelbeyerle, P. Finckh, *Chem. Phys. Lett.* **1987**, *138*, 237–243.
[52] S. N. Helambe, A. Chaudhari, S. C. Mehrotra, *J. Mol. Liq.* **2000**, *84*, 235–244.
[53] J. Barthel, R. Buchner, B. Wurm, *J. Mol. Liq.* **2002**, *98–99*, 51–69.

Received: July 22, 2004
Published online: December 2, 2004

